

See discussions, stats, and author profiles for this publication at: <https://www.researchgate.net/publication/277353255>

Thinking Outside the Cage: Controlling the Extrinsic Porosity and Gas Uptake Properties of Shape Persistent Molecular Cages in Nanoporous Polymers

ARTICLE *in* CHEMISTRY OF MATERIALS · MAY 2015

Impact Factor: 8.35 · DOI: 10.1021/acs.chemmater.5b01346

CITATION

1

READS

67

3 AUTHORS:



[Onur Buyukcakir](#)

Korea Advanced Institute of Science and Tech...

19 PUBLICATIONS 693 CITATIONS

[SEE PROFILE](#)



[Yongbeom Seo](#)

Institute for Basic Science

20 PUBLICATIONS 562 CITATIONS

[SEE PROFILE](#)



[Ali Coskun](#)

Korea Advanced Institute of Science and Tech...

64 PUBLICATIONS 3,137 CITATIONS

[SEE PROFILE](#)

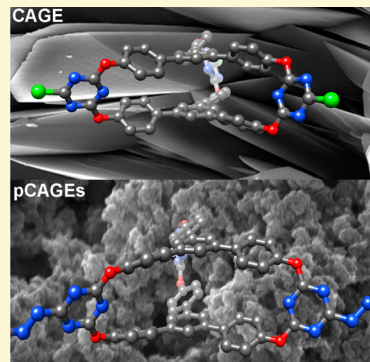
Thinking Outside the Cage: Controlling the Extrinsic Porosity and Gas Uptake Properties of Shape-Persistent Molecular Cages in Nanoporous Polymers

Onur Buyukcakir,[†] Yongbeom Seo,[‡] and Ali Coskun^{*,†,§}

[†]Graduate School of Energy, Environment, Water and Sustainability (EEWS), [‡]Center for Nanomaterials and Chemical Reactions, Institute for Basic Science (IBS), and [§]Department of Chemistry, Korea Advanced Institute of Science and Technology (KAIST), 373-1 Guseong Dong, Daejeon 305-701, Republic of Korea

Supporting Information

ABSTRACT: We present a new strategy to introduce local-order into amorphous nanoporous polymers using shape-persistent organic cage compounds as molecular building blocks in the synthesis of porous cage frameworks (pCAGEs) without any metal catalyst under environmentally benign conditions. We have demonstrated that by varying the size and dimension of the organic linkers extrinsic porosity of organic cages within nanoporous polymers can be controlled, thus allowing us to tune the surface area and gas uptake properties of amorphous pCAGEs. pCAGEs ($SA_{BET} = 628.7\text{--}844.3\text{ m}^2\text{ g}^{-1}$) revealed significantly high CO_2 uptake capacities (up to 4.21 mmol g^{-1} at 1 bar, 273 K) with prominent CO_2/N_2 IAST selectivities (up to 100). Unlike previously reported triazine-based polymers, pCAGEs showed exceptional isosteric heats of adsorption (Q_{st}) values up to 42.9 kJ mol^{-1} for CO_2 at high loading. We attribute the high affinity of CAGE toward CO_2 to the presence of a “cage effect” arising from ultramicroporosity (intrinsic porosity) of CAGE monomers. To prove the cage effect, we have synthesized a control polymer incorporating half-CAGEs as monomeric units. The resulting polymer showed substantially lower Q_{st} values compared to the CAGE and pCAGEs indicating the presence of the cage effect. In addition, the control over the surface area in the case of control polymer was lost completely, thus showing the importance of CAGE monomers as building blocks and the resulting local-order.



1. INTRODUCTION

Ever-increasing CO_2 emissions into the atmosphere and its resulting environmental impact¹ positioned CO_2 capture technologies as an integral part of today's energy industry.^{2–5} Current amine scrubbing technologies for CO_2 capture, however, are quite inefficient as they result in costly energy penalties and degradation of amines along with their corrosive effects.⁶ To date, in order to develop alternative, efficient CO_2 capture platforms, a great number of porous materials, including zeolites,⁷ metal–organic frameworks (MOFs),^{2–5,8} covalent organic frameworks (COFs),^{9–11} and nanoporous polymers^{12–14} have been prepared. In recent years, however, besides these extended porous networks, organic cage compounds have emerged as a new class of porous materials since their first reports by Atwood¹⁵ and Cooper¹⁶ in 2009 as amorphous and crystalline porous materials, respectively. Unlike metal-coordination cages, a limited number of purely organic cage compounds that are synthesized under kinetically controlled reaction conditions have been reported mainly due to their multistep synthesis and low overall yields.¹⁷ These problems were partly overcome by taking advantage of dynamic covalent chemistry (DCC), which opened up new perspectives to construct shape-persistent cage compounds by means of reversible covalent bond formation such as Schiff base chemistry or boronic ester formation. By using DCC,

Cooper,^{16,18–26} Mastalerz,^{17,27–35} Warmuth,³⁶ Gawronski,³⁷ Severin,³⁸ and Zhang^{39,40} have elegantly demonstrated the preparation and gas sorption properties of several interesting cage structures starting from simple precursors in high yields. These cages have already found¹⁷ applications in gas storage,^{28,32,41} separation,^{42,43} and sensing.²⁹ Low hydrolytic stability of organic cage compounds formed using DCC is still a significant challenge, which limits their application as CO_2 capture and separation materials. While an imine-based porous organic cage reported by Cooper et al.²² showed some stability toward humidity under neutral conditions, the stability of these types of cages could be further increased upon reduction of imine linkages. This approach,^{23,28,29,39,44} however, resulted in a loss of rigidity and consequent pore collapse, thus decreasing their surface area. More recently, Cooper et al.²⁴ have shown that postfunctionalization of these reduced cages by the so-called “tying” approach could address not only the flexibility problem, but also the chemical stability.

The porosity of organic cage compounds arises from their internal cavity (intrinsic porosity) and other solvent accessible voids between cage units resulting from packing of cages

Received: April 12, 2015

Revised: May 13, 2015

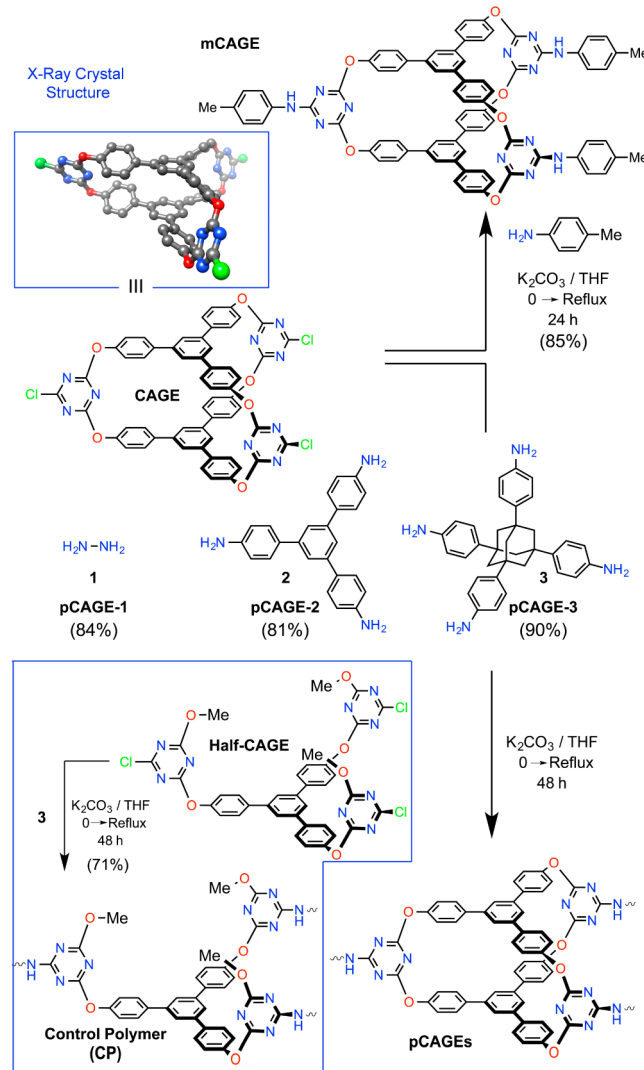
Published: May 13, 2015

(extrinsic porosity). Therefore, the packing mode of cage units plays a crucial role in the determination of their porosity.¹⁸ Moreover, different polymorph formations have already been shown to produce different porosity and surface areas by Cooper^{16,23,24} and Mastalerz.^{32,33} More recently, Doonan et al.⁴⁵ have elegantly demonstrated how two different polymorphs of the same cage compound show completely different BET surface areas: while one of the polymorphs was found to be completely nonporous, the other one had BET surface area of $1153 \text{ m}^2 \text{ g}^{-1}$. Although this polymorphism effect paves the way for the preparation of porous materials with on/off switchable porosity,³³ this drastic change in surface area between different polymorphs is a big disadvantage for practical applications, since the control of polymorphism is an extremely challenging process especially in bulk quantities. The removal of enclathrated solvent is another important parameter, which plays a crucial role in the resulting porosity of the material. Generally, thermal treatment is used to activate the porous materials. However, when this type of activation is applied, most porous cage compounds have either collapsed and became nonporous or their crystal morphology has changed due to thermal stress, which in turn altered their porosity.³⁰ One strategy to overcome these problems is to utilize organic cage compounds as monomeric units to form porous cage frameworks. Although there were few initial efforts to use cage units to build such frameworks, which showed good CO_2/N_2 selectivities, their CO_2 adsorption capacities (up to 0.36 mmol g^{-1} , 1 bar, 293 K) and surface areas (less than $10 \text{ m}^2 \text{ g}^{-1}$) were found to be extremely low for any gas capture or separation application, presumably due to the collapse of the pores of flexible cage monomers and/or unwanted side reactions where the intrinsic pores of cage units were blocked by other monomers.^{40,44} Herein, we not only present (Scheme 1) a new, highly CO_2 -philic organic cage compound, CAGE, but also introduce a catalyst-free, efficient polymerization route to construct porous cage frameworks (pCAGEs) by reacting shape-persistent cage molecules with different organic linkers under environmentally benign conditions. We have demonstrated that by simply varying the size of the linker the extrinsic porosity of organic cages within nanoporous polymers can be controlled, thus allowing us to tune the surface area of amorphous pCAGEs (S_{BET} between 628.7 and $844.3 \text{ m}^2 \text{ g}^{-1}$). Moreover, these cage frameworks showed remarkable CO_2 gas uptake capacities (up to 4.21 mmol g^{-1} at 1 bar, 273 K) and high CO_2/N_2 selectivities (up to 100, at 1 bar, 273 K). In addition, this strategy also allowed us to introduce local-order into amorphous nanoporous polymers and increase the predictability of their structure by incorporating well-defined organic cages with intrinsic porosity. We have also introduced the so-called “cage effect”; that is, CO_2 molecules located within the intrinsic pores of cage experience higher binding affinity (isosteric heat of adsorption, Q_{st} , up to 42.9 kJ mol^{-1}) via dipole–quadrupole interactions between triazine nitrogens and CO_2 molecules, in nanoporous polymers.

2. EXPERIMENTAL SECTION

2.1. General Synthetic Procedure for pCAGEs and CP. In a typical reaction, CAGE or half-CAGE was dissolved in anhydrous THF at room temperature, followed by the addition of finely ground K_2CO_3 . The reaction mixture was cooled down to 0°C , and the corresponding amine ($-\text{Cl}$: $-\text{NH}_2$, 1:1 stoichiometry) was slowly added under argon atmosphere. Then, the reaction mixture was stirred at 0°C for 12 h, at room temperature for 18 h, and finally under reflux

Scheme 1. Structural Formulas of CAGE and Half-CAGE and the Synthesis of Model Cage Compound (mCAGE), Porous Cage Frameworks (pCAGEs), and the Control Polymer (CP)



conditions for 18 h. After the reaction mixture cooled to room temperature, it was filtered with a fine fritted funnel and washed with THF ($2 \times 100 \text{ mL}$) and deionized water ($2 \times 100 \text{ mL}$). Then, the resulting white powder was extensively washed with THF ($3 \times 200 \text{ mL}$), acetone ($3 \times 200 \text{ mL}$), and diethyl ether ($3 \times 200 \text{ mL}$). The white powder was dried at room temperature under vacuum for 24 h to give the product.

2.2. Measurements. ^1H and ^{13}C spectra were recorded on Bruker Avance 300 MHz NMR and Agilent 400 MHz NMR spectrometers at ambient temperature. Solid-state cross-polarization magic angle spinning (CP/MAS) ^{13}C NMR spectra of polymers were recorded on a Bruker Digital Avance III HD 400 WB (400 MHz) NMR spectrometer at ambient temperature with a magic angle spinning rate of 7.0 kHz. FT-IR spectra were recorded in ATR mode by using a Shimadzu FT-IR spectrometer. Thermogravimetric analysis (TGA) was performed by using a NETZSCH-TG 209 F3 instrument, and the samples were heated to 800°C at a rate of $10^\circ\text{C min}^{-1}$ under air and N_2 atmosphere for each sample. The scanning electron microscopy (SEM) analyses were performed using Hitachi S-4800 FE-SEM at 2.0–10 kV. Elemental analyses (C, H, N) were recorded on a FlashEA 2000 (Series) [C,H,N,S] elemental analyzer. Powder X-ray Diffraction (PXRD) analyses of samples were carried out over the 2θ range of 5° to 80° on a Bruker AXS D8 Discover multipurpose high power X-ray

diffractometer. The surface area and pore size distribution analysis of samples were performed with a Micrometrics 3Flex Surface Characterization Analyzer by argon adsorption and desorption at 87 K. All the samples were degassed at 100 °C for 6 h under vacuum prior to the analysis. The surface areas of samples were calculated using the BET and Langmuir model in the pressure range where the term $V(1 - P/P_0)$ continuously increases with P/P_0 in the Rouquerol plot. The pore size distributions of samples were calculated from argon isotherms according to nonlocal density functional theory (NLDFT) method using a zeolite cylindrical pore model. The low-pressure CO₂ and N₂ adsorption isotherms of samples were taken at two different temperatures, 273 and 298 K. The samples were also degassed before the adsorption analysis at 100 °C for 6 h under vacuum. The circulator was used to keep the temperature constant during adsorption/desorption analysis. The CO₂/N₂ selectivity was calculated by using ideal adsorbed solution theory (IAST) from the CO₂ and N₂ adsorption isotherms at the corresponding temperatures (273 and 298 K), which is calculated by means of OriginPro v8.5. Isosteric heat of absorption (Q_s) values were calculated by using the standard calculation routine, that is, the Clausius–Clapeyron equation, in the data master offline data reduction software (Micrometrics).

3. RESULTS AND DISCUSSION

3.1. Synthesis. The CAGE compound was synthesized (Scheme 1)⁴⁶ by reacting 1,3,5-tri(*p*-hydroxyphenyl)benzene with cyanuric chloride in two steps with 38% yield for the cage formation. Reactivity differences of chloro atoms toward nucleophilic aromatic substitution on cyanuric chloride allowed us to synthesize CAGE compound in a controlled manner. Reaction of 1,3,5-tri(*p*-hydroxyphenyl)benzene with cyanuric chloride at 0 °C was followed by the cage formation step at room temperature. We have also synthesized a half-CAGE by reacting 1,3,5-tri(*p*-hydroxyphenyl)benzene with 2,4-dichloro-6-methoxy-1,3,5-triazine.⁴⁶ As the final chloride atom on the CAGE and half-CAGE can be reacted at above 60 °C, it can be readily polymerized to form pCAGEs and control polymer (CP) without any metal catalyst. In order to test our hypothesis and check the stability of CAGE in the presence of nucleophiles, we first reacted CAGE with *p*-toluidine in the presence of K₂CO₃ in THF under reflux conditions for 24 h. The corresponding model CAGE (mCAGE) compound was obtained successfully in 85% yield and characterized (see Supporting Information, SI) using ¹H NMR, ¹³C NMR, and high-resolution mass spectroscopy. For the polymerization reactions of CAGE, we have identified three different organic linkers with different size and dimensions, namely, hydrazine (1D), 1,3,5-tri(4-aminophenyl) benzene (2D), and tetrakis(4-aminophenyl)adamantane (3D), to construct pCAGE-1, pCAGE-2, and pCAGE-3, respectively (Scheme 1). As for the synthesis of CP, we have reacted half-CAGE with tetrakis(4-aminophenyl)adamantane. We have carried out the polymerization reactions by gradually increasing reaction temperature in order to get more uniform pore formation.

3.2. Spectroscopic Characterization. CAGE, mCAGE, CP, and pCAGEs were characterized using solid-state cross-polarization magic-angle spinning (CP-MAS) ¹³C NMR, scanning electron microscopy (SEM), powder X-ray diffraction (PXRD), FT-IR spectroscopy, thermogravimetric analysis (TGA), and elemental analysis (EA) (see Supporting Information). The formation of polymers was first verified (Figure 1) by using CP-MAS ¹³C NMR. The carbon peaks of the triazine moiety located at 172 ppm were broadened and split into two peaks, indicating the formation of pCAGEs. This result is also in perfect agreement with the solid-state ¹³C NMR spectrum of the mCAGE (Figure 1). It is important to note

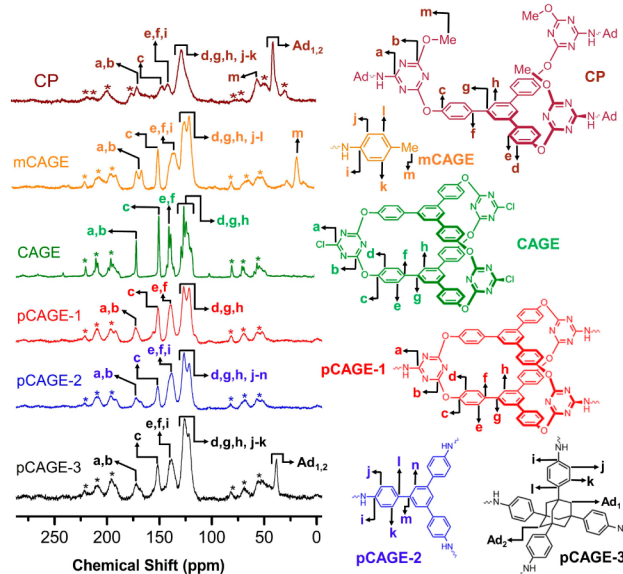


Figure 1. CP-MAS ¹³C NMR spectra of CAGE, mCAGE, CP, and pCAGEs and corresponding peak assignments. The spectra were recorded with a contact time of 2 ms, a relaxation time of 5 s, and a spinning frequency of 7 kHz. The carbonyl carbon of glycine was used as an external chemical shift reference for the ¹³C NMR. * denotes spinning side bands.

that carbon peaks associated with the 1,3,5-triphenylbenzene moiety within the CAGE broadened due to polymerization for all pCAGEs, showing that CAGE monomer was successfully incorporated into the pCAGE backbone. Splitting of triazine carbons in CP along with carbon peaks associated with adamantane also verifies successful introduction of half-CAGE units into the polymer backbone. In order to analyze bulk scale morphology of the CAGE and mCAGE crystals, CP and pCAGEs, we have carried out (Figure 2 and Supporting

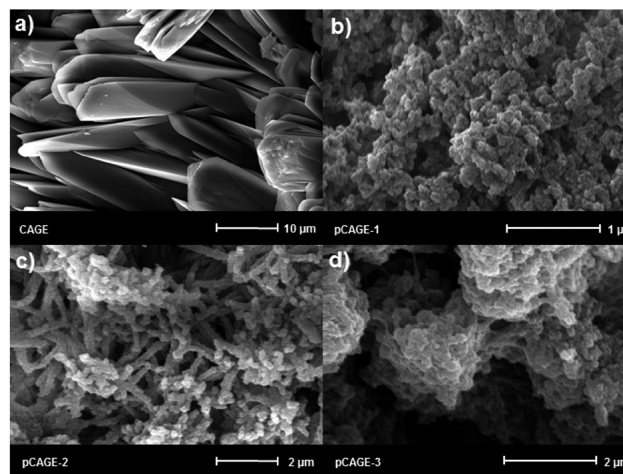


Figure 2. Scanning electron microscopy (SEM) images of CAGE and pCAGEs: CAGE (a), pCAGE-1 (b), pCAGE-2 (c), pCAGE-3 (d).

Information Figure S1) SEM analysis. Flake-like micron-sized crystals of CAGE are clearly visible in Figure 2a. Following their polymerization, however, CAGE crystals experienced significant morphology changes. While pCAGE-1 formed uniform spherical particles, pCAGE-2 showed a worm-like morphology. On the contrary, pCAGE-3 formed spongey agglomerated

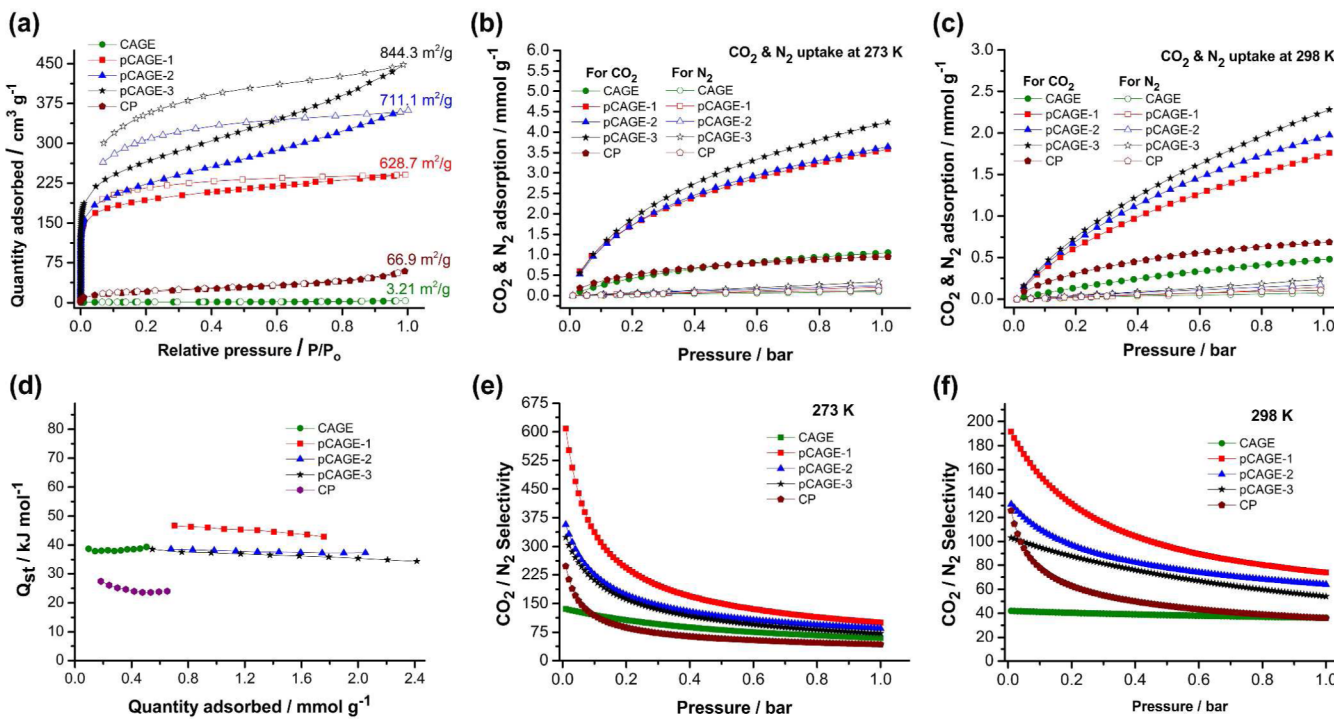


Figure 3. Argon uptake isotherms of CAGE, pCAGEs, and control polymer (CP) at 87 K (a). Filled and empty symbols represent adsorption and desorption, respectively. CO₂ and N₂ uptake isotherms of CAGE, pCAGEs, and CP measured up to 1 bar at 273 K (b) and 298 K (c). Isosteric heats of adsorption (Q_{st}) of CO₂ for CAGE, pCAGEs, and CP (d). CO₂/N₂ selectivity of CAGE, pCAGEs, and CP measured by IAST technique for mole ratio of 15:85 gas mixture of CO₂/N₂ at 273 K (e) and 298 K (f).

Table 1. CO₂ and N₂ Uptakes, Selectivities, Isosteric Heats of Adsorptions and BET/Langmuir Surface Areas of CAGE, pCAGEs, and Control Polymer (CP)

polymer	BET, ^a Ar ($\text{m}^2 \text{g}^{-1}$)	Langmuir ($\text{m}^2 \text{g}^{-1}$)	CO ₂ adsorption (mmol g ⁻¹)		N ₂ adsorption (mmol g ⁻¹)		CO ₂ /N ₂ (15:85) at 1 bar ^b		Q _{st} for CO ₂ (kJ mol ⁻¹)	
			273 K	298 K	273 K	298 K	273 K	298 K	zero coverage	high loading
CAGE	3.2 (132) ^c	8.2	1.04	0.48	0.10	0.07	59.9	36.3	38.8	39.4
pCAGE-1	628.7	881.3	3.55	1.75	0.21	0.14	100.1	73.8	46.6	42.9
pCAGE-2	711.1	1228.8	3.62	1.96	0.24	0.17	84.7	64.0	38.7	37.3
pCAGE-3	844.3	1491.6	4.21	2.26	0.34	0.24	72.2	54.1	38.6	34.4
CP	66.9	160.6	0.95	0.68	0.12	0.10	42.7	35.9	27.4	25.2

^aCalculated according to the Rouquerol plots. ^bFrom IAST at CO₂:N₂ ratio of 0.15:0.85 at 1 bar. ^cCalculated from the CO₂ adsorption isotherm at 273 K.

structures. In addition, CP also showed similar superstructures to that of pCAGE-3. In order to further verify the crystallinity of CAGE, we have also carried out (Supporting Information Figure S2) PXRD analysis. CAGE crystals were obtained by fast precipitation technique by addition of diethyl ether to the THF solution of CAGE. Impressively, precipitated crystals of CAGE were still in crystalline state with the same morphology as that of single crystals of CAGE and in good agreement with the simulated PXRD spectrum with slight loss of crystallinity presumably due to thermal activation at 100 °C. The CAGE monomer exhibited average interplane distance of 4.1 Å, which is very close to ultramicroporous MOFs (3.84 Å) reported by Eddaoudi et al.,⁴⁷ between two central benzene rings.⁴⁶ Although pCAGEs have amorphous character, they still show broad diffraction peaks corresponding to CAGE structure, which further verifies successful incorporation of CAGE units into pCAGEs. As expected, we did not observe these broad features in the case of CP, which was found to be completely amorphous. In order to show thermal stability of CAGE, CP,

and pCAGEs, we have carried out TGA analysis; CAGE, CP, and pCAGEs showed (Supporting Information Figure S3) excellent thermal stability in air up to 420 °C and in N₂ atmosphere up to 450 °C. The weight loss below 200 °C is attributed to the removal of trapped solvents and moisture.

3.3. Gas Sorption Studies. The porosities of CAGE, CP, and pCAGEs were investigated (Figure 3a) by argon adsorption–desorption isotherms at 87 K, showing a reversible type I isotherm. Significant adsorption at low pressure and also observed type H4 hysteresis for desorption were attributed to the microporosity and swelling of the framework. All samples were activated at 100 °C for 6 h prior to the gas uptake measurements in order to remove trapped gases, solvent molecules, and moisture. The surface areas of CAGE, CP, and pCAGEs, estimated from the argon adsorption isotherm using the Brunauer–Emmett–Teller (BET) model, in which the pressure ranges were determined according to the Rouquerol plots (Supporting Information Figures S4 and S5), were found (Table 1) to be 3.2, 628.7, 711.1, 844.3, and 66.9 m^2/g for

CAGE, pCAGE-1, pCAGE-2, pCAGE-3, CP, respectively. The median pore width was found (Supporting Information Figure S6) to be 5.1, 8.0, and 8.6 Å for pCAGE-1, pCAGE-2 and pCAGE-3, respectively. The pore size distributions (PSDs) were calculated from argon adsorption isotherms by using NLDFT zeolite cylindrical pore model (in perfect agreement with the calculated isotherms, Supporting Information Figure S7), and pCAGEs showed narrow PSDs mainly in the micropore range. The increasing size and dimension of organic linkers lead to an increase in both surface area and median pore width of pCAGEs due to an increase in the extrinsic porosity, which is proportional to size of the organic linkers, within pCAGEs. Moreover, the local-order introduced by the CAGE monomers and their size also contributed to the control over surface area by decreasing over interpenetration during polymerization reaction. In the case of CP, however, the control over the surface area was lost completely, thus showing the importance of CAGE monomers as building blocks and the resulting local-order. We attribute this effect to the size of CAGE units, which limits interpenetration of the framework, thus leading to higher surface area when compared to the CP.

We have also investigated (Figure 3b,c) the CO₂ and N₂ uptake of CAGE, CP, and pCAGEs up to 1 bar at 273 and 298 K in order to measure their gas uptake capacity. In spite of its relatively low surface area, CAGE showed significant CO₂ uptake capacity of 1.04 and 0.48 mmol g⁻¹ at 273 and 298 K (1 bar), respectively. This result prompted us to investigate the CO₂ surface area of CAGE at 273 K. CO₂ surface area of CAGE was found (Supporting Information Figure S8) to be 132 m² g⁻¹, an indication of high affinity of CO₂ toward CAGE and also accessibility of CO₂ into the intrinsic pores of the CAGE units. High affinity of CO₂ can be further verified by the isosteric heats of adsorption (Q_{st}) data, which were calculated (Figure 3d) from the CO₂ adsorption data at 273 and 298 K. The Q_{st} value of CO₂ adsorption for CAGE was found to be 39.4 kJ mol⁻¹ at high loading, which is one of the highest Q_{st} values reported to date for physisorption on microporous solids. Lack of hysteresis in CO₂ adsorption–desorption isotherms of CAGE and pCAGEs further confirmed (Supporting Information Figure S9) the physisorption mechanism. Q_{st} values of CAGE and pCAGEs were also found to be higher compared to that of other nanoporous polymers incorporating triazine moieties (24.5–31 kJ mol⁻¹ at high loadings) regardless of their surface areas and CO₂ uptake capacities (for detailed comparison of triazine containing porous polymers, see Supporting Information Table S1),^{48–50} pointing to the fact that there is a significant “cage effect” arising from ultramicropores of cage units. This effect was further proven by measuring CO₂ uptake capacity and calculating the corresponding Q_{st} value for CP. CP showed CO₂ uptake capacity of 0.95 and 0.68 mmol g⁻¹ at 273 and 298 K, respectively, with a Q_{st} value of 25.2 kJ mol⁻¹ calculated from the CO₂ adsorption data at 273 and 298 K. Although CP had additional nitrogen atoms in its structure and higher nitrogen content compared to both CAGE and pCAGEs based on EA data, it showed 11.4 kJ mol⁻¹ lower Q_{st} value for CO₂ adsorption when compared to that of CAGE and pCAGEs at zero coverage (Table 1). It is also important to note that CAGE and pCAGEs showed similar Q_{st} values at zero coverage, thus proving the critical role of CAGE cavity for high CO₂ affinity. We believe that the intrinsic pores of CAGE units act like ultramicropores, which in turn significantly increase the resulting Q_{st} value. Evidently, a similar ultramicroporosity effect in MOFs was recently reported by

Eddaoudi et al.⁴⁷ They elegantly demonstrated that ultramicroporous MOFs with pore diameter of 3.84 Å exhibit Q_{st} value of 45 kJ mol⁻¹ for CO₂; however, when the pore diameter is increased to 5.15 Å, the Q_{st} value becomes 31.9 kJ mol⁻¹. Our Q_{st} values are slightly lower when compared to this Zn-based MOF with 3.84 Å pore diameter presumably due to relatively larger cavity of cage units (4.1 Å) along with the presence of extrinsic pores in the polymer structure. It is important to note that although pCAGEs had much higher surface areas compared to CP, they still showed higher Q_{st} values for CO₂ demonstrating clearly the effect of CAGE units (Table 1) as the low surface area polymers usually exhibit higher Q_{st} values mainly due to the interpenetration of the framework, wherein gas molecules can interact with more than one functional group.

Upon polymerization of CAGE, although the resulting polymer became amorphous, accessibility of both intrinsic and extrinsic pores for gas molecules increased substantially. As expected, increasing surface area resulted in an increase in CO₂ uptake capacity. pCAGE-1 and pCAGE-2 showed remarkable CO₂ uptake capacities of 3.55 and 3.62 mmol g⁻¹ (at 1 bar, 273 K), respectively. pCAGE-3 revealed the highest CO₂ uptake of 4.21 mmol g⁻¹ at 273 K, 1 bar among all pCAGEs. Moreover, pCAGEs still showed significant CO₂ uptakes at 298 K; we found 1.75, 1.96, and 2.26 mmol g⁻¹ for pCAGE-1–3, respectively. We have calculated Q_{st} values of 42.9, 37.3, and 34.4 kJ mol⁻¹ (at zero coverage, 46.6, 38.7, 38.6 kJ mol⁻¹) at high loading for pCAGE-1, -2, and -3, respectively. Increase in CO₂ uptake capacity with increasing surface area was accompanied by a decrease in Q_{st} values. Since increasing the size of organic linker will decrease the CAGE concentration in the polymer, resulting cage effect and ultramicroporosity should also decrease, thus leading to relatively lower Q_{st} values. Higher Q_{st} value of pCAGE-1 (42.9 kJ mol⁻¹), which is slightly off the trend, can be explained by the presence of highly acidic N–H protons, which can form hydrogen bonding interactions with CO₂ gas molecules.⁵¹ Although the CO₂ uptake capacities of pCAGE-1 and -2 are close to each other at 273 K due to the hydrogen bonding effect associated with hydrazine protons, the difference becomes larger at 298 K, as the hydrogen bonding interactions will be less effective at higher temperatures. A similar trend was also observed for N₂ gas, as the cage concentration decreased going from CAGE to pCAGE-3, and N₂ uptake increased.

3.4. Gas Selectivity. In order to simulate flue gas conditions, we have calculated (Figure 3e,f and Table 1) CO₂/N₂ selectivity for CAGE, CP, and pCAGEs from the CO₂ and N₂ adsorption isotherms using ideal adsorbed solution theory (IAST) for CO₂:N₂ mixture (15:85) at two different temperatures, 273 and 298 K (Table 1). For postcombustion CO₂ capture, porous sorbents should show high gas uptake capacities while retaining their high CO₂/N₂ selectivity. We found IAST values of 59.9, 100.1, 84.7, 72.2, and 42.7 for CAGE, pCAGE-1–3, and CP at 273 K, respectively. As expected, CAGE, CP, and pCAGEs showed decreasing selectivity with increasing temperature mainly due to the loss of affinity of gas molecules toward the binding sites. Since the polymerization of CAGE into pCAGEs allowed us to increase the accessibility of both intrinsic and extrinsic pores while retaining unique properties of CAGE, we observed a CO₂/N₂ selectivity increase from 59.9 to 100.1, by simply converting CAGE into pCAGE-1. We believe that additional hydrogen bonding interactions between hydrazine linkage and CO₂

molecules in pCAGE-1 also contributed to this selectivity increase. Clearly, a high concentration of CAGE units within pCAGEs is critical for high CO₂/N₂ selectivity as also verified by CP. Upon an increase in the size of the organic linker in pCAGE-2 and -3, selectivity decreased to 84.7 and 72.2, respectively. It is important to note that, by taking advantage of local-order introduced into pCAGEs by using CAGE as a monomer, we can not only control the surface area and gas uptake, but also the CO₂/N₂ selectivity of pCAGEs.

4. CONCLUSION

We have demonstrated, for the first time, by introducing local-order, using shape-persistent organic cage compounds with intrinsic porosity, into amorphous nanoporous polymers, we can not only control gas sorption properties of these polymers, but also increase the predictability of their structure and properties. We have also introduced the so-called “cage effect” arising from ultramicropores of cage units, which provides higher binding affinity between gas molecules and binding sites within cage units. Apart from gas storage and separation, applications including sensing and host–guest chemistry are also promising with pGAGEs, which possess binary characteristics of shape-persistent organic cages and amorphous nanoporous polymers. We also believe that these findings will help to bridge the gap between crystalline organic cage compounds and amorphous polymers, contribute to the development of porous polymers with tunable properties, and bring a new perspective for the preparation of porous materials in general.

■ ASSOCIATED CONTENT

S Supporting Information

Experimental details and additional spectroscopic characterization data. The Supporting Information is available free of charge on the ACS Publications website at DOI: 10.1021/acs.chemmater.5b01346.

■ AUTHOR INFORMATION

Corresponding Author

*E-mail: coskun@kaist.ac.kr. Fax: +82 42 350 2248. Phone: +82 42 350 1724.

Notes

The authors declare no competing financial interest.

■ ACKNOWLEDGMENTS

We acknowledge support from the Basic Science Research Program through the National Research Foundation of Korea (NRF) funded by the Ministry of Science, ICT & Future Planning (2013R1A1A1012282). This work was also partially supported by the National Research Foundation of Korea (NRF) Grant funded by the Korea government (MEST) (NRF-2014R1A4A1003712 and BK21 PLUS program). The authors wish to thank Prof. Ryong Ryoo for access to the solid state NMR spectroscopy (IBS, Daejeon, Korea).

■ REFERENCES

- (1) Monastersky, R. Global carbon dioxide levels near worrisome milestone. *Nature* **2013**, *497*, 13–14.
- (2) Lee, J.; Farha, O. K.; Roberts, J.; Scheidt, K. A.; Nguyen, S. T.; Hupp, J. T. Metal-organic framework materials as catalysts. *Chem. Soc. Rev.* **2009**, *38*, 1450–1459.
- (3) MacDowell, N.; Florin, N.; Buchard, A.; Hallett, J.; Galindo, A.; Jackson, G.; Adjiman, C. S.; Williams, C. K.; Shah, N.; Fennell, P. An overview of CO₂ capture technologies. *Energy Environ. Sci.* **2010**, *3*, 1645–1669.
- (4) D’Alessandro, D. M.; Smit, B.; Long, J. R. Carbon dioxide capture: Prospects for new materials. *Angew. Chem., Int. Ed.* **2010**, *49*, 6058–6082.
- (5) Kenarsari, S. D.; Yang, D.; Jiang, G.; Zhang, S.; Wang, J.; Russell, A. G.; Wei, Q.; Fan, M. Review of recent advances in carbon dioxide separation and capture. *RSC Adv.* **2013**, *3*, 22739–22773.
- (6) Rochelle, G. T. Amine scrubbing for CO₂ capture. *Science* **2009**, *325*, 1652–1654.
- (7) Cheung, O.; Hedin, N. Zeolites and related sorbents with narrow pores for CO₂ separation from flue gas. *RSC Adv.* **2014**, *4*, 14480–14494.
- (8) Furukawa, H.; Cordova, K. E.; O’Keeffe, M.; Yaghi, O. M. The chemistry and applications of metal-organic frameworks. *Science* **2013**, *341*.
- (9) Ding, S.-Y.; Wang, W. Covalent organic frameworks (COFs): from design to applications. *Chem. Soc. Rev.* **2013**, *42*, 548–568.
- (10) Colson, J. W.; Dichtel, W. R. Rationally synthesized two-dimensional polymers. *Nat. Chem.* **2013**, *5*, 453–465.
- (11) El-Kaderi, H. M.; Hunt, J. R.; Mendoza-Cortés, J. L.; Côté, A. P.; Taylor, R. E.; O’Keeffe, M.; Yaghi, O. M. Designed synthesis of 3D covalent organic frameworks. *Science* **2007**, *316*, 268–272.
- (12) Thomas, A. Functional materials: From hard to soft porous frameworks. *Angew. Chem., Int. Ed.* **2010**, *49*, 8328–8344.
- (13) McKeown, N. B.; Budd, P. M. Exploitation of intrinsic microporosity in polymer-based materials. *Macromolecules* **2010**, *43*, 5163–5176.
- (14) Dawson, R.; Cooper, A. I.; Adams, D. J. Nanoporous organic polymer networks. *Prog. Polym. Sci.* **2012**, *37*, 530–563.
- (15) Tian, J.; Thallapally, P. K.; Dalgarno, S. J.; McGrail, P. B.; Atwood, J. L. Amorphous molecular organic solids for gas adsorption. *Angew. Chem., Int. Ed.* **2009**, *48*, 5492–5495.
- (16) Tozawa, T.; Jones, J. T. A.; Swamy, S. I.; Jiang, S.; Adams, D. J.; Shakespeare, S.; Clowes, R.; Bradshaw, D.; Hasell, T.; Chong, S. Y.; Tang, C.; Thompson, S.; Parker, J.; Trewin, A.; Bacsa, J.; Slawin, A. M. Z.; Steiner, A.; Cooper, A. I. Porous organic cages. *Nat. Mater.* **2009**, *8*, 973–978.
- (17) Zhang, G.; Mastalerz, M. Organic cage compounds—from shape-persistent to function. *Chem. Soc. Rev.* **2014**, *43*, 1934–1947.
- (18) Bojdys, M. J.; Briggs, M. E.; Jones, J. T. A.; Adams, D. J.; Chong, S. Y.; Schmidtmann, M.; Cooper, A. I. Supramolecular engineering of intrinsic and extrinsic porosity in covalent organic cages. *J. Am. Chem. Soc.* **2011**, *133*, 16566–16571.
- (19) Cooper, A. I. Nanoporous organics enter the cage age. *Angew. Chem., Int. Ed.* **2011**, *50*, 996–998.
- (20) Hasell, T.; Chong, S. Y.; Jelfs, K. E.; Adams, D. J.; Cooper, A. I. Porous organic cage nanocrystals by solution mixing. *J. Am. Chem. Soc.* **2011**, *134*, 588–598.
- (21) Jones, J. T. A.; Hasell, T.; Wu, X.; Bacsa, J.; Jelfs, K. E.; Schmidtmann, M.; Chong, S. Y.; Adams, D. J.; Trewin, A.; Schiffman, F.; Cora, F.; Slater, B.; Steiner, A.; Day, G. M.; Cooper, A. I. Modular and predictable assembly of porous organic molecular crystals. *Nature* **2011**, *474*, 367–371.
- (22) Hasell, T.; Schmidtmann, M.; Stone, C. A.; Smith, M. W.; Cooper, A. I. Reversible water uptake by a stable imine-based porous organic cage. *Chem. Commun.* **2012**, *48*, 4689–4691.
- (23) Culshaw, J. L.; Cheng, G.; Schmidtmann, M.; Hasell, T.; Liu, M.; Adams, D. J.; Cooper, A. I. Dodecaamide cages: Organic 12-arm building blocks for supramolecular chemistry. *J. Am. Chem. Soc.* **2013**, *135*, 10007–10010.
- (24) Liu, M.; Little, M. A.; Jelfs, K. E.; Jones, J. T. A.; Schmidtmann, M.; Chong, S. Y.; Hasell, T.; Cooper, A. I. Acid- and base-stable porous organic cages: Shape persistence and pH stability via post-synthetic “tying” of a flexible amine cage. *J. Am. Chem. Soc.* **2014**, *136*, 7583–7586.
- (25) Mitra, T.; Jelfs, K. E.; Schmidtmann, M.; Ahmed, A.; Chong, S. Y.; Adams, D. J.; Cooper, A. I. Molecular shape sorting using molecular organic cages. *Nat. Chem.* **2013**, *5*, 276–281.

- (26) Hasell, T.; Zhang, H.; Cooper, A. I. Solution-processable molecular cage micropores for hierarchically porous materials. *Adv. Mater.* **2012**, *24*, 5732–5737.
- (27) Mastalerz, M. Shape-persistent organic cage compounds by dynamic covalent bond formation. *Angew. Chem., Int. Ed.* **2010**, *49*, 5042–5053.
- (28) Mastalerz, M.; Schneider, M. W.; Oppel, I. M.; Presly, O. A Salicylbisimine cage compound with high surface area and selective CO_2/CH_4 adsorption. *Angew. Chem., Int. Ed.* **2011**, *50*, 1046–1051.
- (29) Brutschy, M.; Schneider, M. W.; Mastalerz, M.; Waldvogel, S. R. Porous organic cage compounds as highly potent affinity materials for sensing by quartz crystal microbalances. *Adv. Mater.* **2012**, *24*, 6049–6052.
- (30) Mastalerz, M. Permanent porous materials from discrete organic molecules—Towards ultra-high surface areas. *Chem.—Eur. J.* **2012**, *18*, 10082–10091.
- (31) Schneider, M. W.; Hauswald, H. J.; Stoll, R.; Mastalerz, M. A shape-persistent exo-functionalized [4 + 6] imine cage compound with a very high specific surface area. *Chem. Commun.* **2012**, *48*, 9861–3.
- (32) Schneider, M. W.; Oppel, I. M.; Mastalerz, M. Exo-functionalized shape-persistent [2 + 3] cage compounds: Influence of molecular rigidity on formation and permanent porosity. *Chem.—Eur. J.* **2012**, *18*, 4156–4160.
- (33) Schneider, M. W.; Oppel, I. M.; Ott, H.; Lechner, L. G.; Hauswald, H. J.; Stoll, R.; Mastalerz, M. Periphery-substituted [4 + 6] salicylbisimine cage compounds with exceptionally high surface areas: Influence of the molecular structure on nitrogen sorption properties. *Chem.—Eur. J.* **2012**, *18*, 836–47.
- (34) Mastalerz, M. Modular synthesis of shape-persistent organic cage compounds: Molecular precursors for a new class of permanent porous materials. *Synlett* **2013**, *24*, 781–786.
- (35) Zhang, G.; Presly, O.; White, F.; Oppel, I. M.; Mastalerz, M. A Permanent mesoporous organic cage with an exceptionally high surface area. *Angew. Chem., Int. Ed.* **2014**, *53*, 1516–1520.
- (36) Liu, X.; Liu, Y.; Li, G.; Warmuth, R. One-pot, 18-component synthesis of an octahedral nanocontainer molecule. *Angew. Chem., Int. Ed.* **2006**, *45*, 901–904.
- (37) Skowronek, P.; Warzajtis, B.; Rychlewska, U.; Gawronski, J. Self-assembly of a covalent organic cage with exceptionally large and symmetrical interior cavity: the role of entropy of symmetry. *Chem. Commun.* **2013**, *49*, 2524–2526.
- (38) Granzhan, A.; Riis-Johannessen, T.; Scopelliti, R.; Severin, K. Combining metallasupramolecular chemistry with dynamic covalent chemistry: Synthesis of large molecular cages. *Angew. Chem., Int. Ed.* **2010**, *49*, 5515–5518.
- (39) Jin, Y.; Voss, B. A.; Noble, R. D.; Zhang, W. A Shape-persistent organic molecular cage with high selectivity for the adsorption of CO_2 over N_2 . *Angew. Chem., Int. Ed.* **2010**, *49*, 6348–6351.
- (40) Jin, Y.; Voss, B. A.; Jin, A.; Long, H.; Noble, R. D.; Zhang, W. Highly CO_2 -selective organic molecular cages: What determines the CO_2 selectivity. *J. Am. Chem. Soc.* **2011**, *133*, 6650–6658.
- (41) Schneider, M. W.; Oppel, I. M.; Griffin, A.; Mastalerz, M. Post-modification of the interior of porous shape-persistent organic cage compounds. *Angew. Chem., Int. Ed.* **2013**, *52*, 3611–3615.
- (42) Chen, L.; Reiss, P. S.; Chong, S. Y.; Holden, D.; Jelfs, K. E.; Hasell, T.; Little, M. A.; Kewley, A.; Briggs, M. E.; Stephenson, A.; Thomas, K. M.; Armstrong, J. A.; Bell, J.; Bustos, J.; Noel, R.; Liu, J.; Strachan, D. M.; Thallapally, P. K.; Cooper, A. I. Separation of rare gases and chiral molecules by selective binding in porous organic cages. *Nat. Mater.* **2014**, *13*, 954–960.
- (43) Bushell, A. F.; Budd, P. M.; Attfield, M. P.; Jones, J. T. A.; Hasell, T.; Cooper, A. I.; Bernardo, P.; Bazzarelli, F.; Clarizia, G.; Jansen, J. C. Nanoporous organic polymer/cage composite membranes. *Angew. Chem., Int. Ed.* **2013**, *52*, 1253–1256.
- (44) Jin, Y.; Voss, B. A.; McCaffrey, R.; Baggett, C. T.; Noble, R. D.; Zhang, W. Microwave-assisted syntheses of highly CO_2 -selective organic cage frameworks (OCFs). *Chem. Sci.* **2012**, *3*, 874–877.
- (45) Avellaneda, A.; Valente, P.; Burgun, A.; Evans, J. D.; Markwell-Heys, A. W.; Rankine, D.; Nielsen, D. J.; Hill, M. R.; Sumby, C. J.; Doonan, C. J. Kinetically controlled porosity in a robust organic cage material. *Angew. Chem., Int. Ed.* **2013**, *52*, 3746–3749.
- (46) Naseer, M. M.; Wang, D.-X.; Zhao, L.; Huang, Z.-T.; Wang, M.-X. Synthesis and functionalization of heteroatom-bridged bicyclocalixaromatics, large molecular triangular prisms with electron-rich and -deficient aromatic interiors. *J. Org. Chem.* **2011**, *76*, 1804–1813.
- (47) Nugent, P.; Belmabkhout, Y.; Burd, S. D.; Cairns, A. J.; Luebke, R.; Forrest, K.; Pham, T.; Ma, S.; Space, B.; Wojtas, L.; Eddaoudi, M.; Zaworotko, M. J. Porous materials with optimal adsorption thermodynamics and kinetics for CO_2 separation. *Nature* **2013**, *495*, 80–84.
- (48) Patel, H. A.; Karadas, F.; Byun, J.; Park, J.; Deniz, E.; Canlier, A.; Jung, Y.; Atilhan, M.; Yavuz, C. T. Highly stable nanoporous sulfur-bridged covalent organic polymers for carbon dioxide removal. *Adv. Funct. Mater.* **2013**, *23*, 2270–2276.
- (49) Zhao, H.; Jin, Z.; Su, H.; Zhang, J.; Yao, X.; Zhao, H.; Zhu, G. Target synthesis of a novel porous aromatic framework and its highly selective separation of CO_2/CH_4 . *Chem. Commun.* **2013**, *49*, 2780–2782.
- (50) Liebl, M. R.; Senker, J. Microporous functionalized triazine-based polyimides with high CO_2 capture capacity. *Chem. Mater.* **2013**, *25*, 970–980.
- (51) Rabbani, M. G.; El-Kaderi, H. M. Template-free synthesis of a highly porous benzimidazole-linked polymer for CO_2 capture and H_2 storage. *Chem. Mater.* **2011**, *23*, 1650–1653.